Theoretical and Applied Climatology (2025) 156:442
https://doi.org/10.1007/s00704-025-05660-3

RESEARCH

Investigation into the causes of surface urban heat islands using an urban canopy model: comparison between bulk and facet approaches

Kyeongjoo Park[1] · **Jong-Jin Baik**[1] · **Han-Gyul Jin**[2,3]

Received: 8 January 2025 / Accepted: 4 July 2025

Abstract

Urban canopy models (UCMs) help to better understand urban climatic phenomena including surface urban heat islands (SUHIs). Previous studies employing UCMs investigated the causes of SUHIs by analyzing surface energy fluxes balanced for an urban conceptual volume (bulk approach). In this approach, since the urban surface energy fluxes are represented at the top surface of the conceptual volume, the representative urban surface temperature is the radiative surface temperature inverted from emitted longwave radiation there. Meanwhile, the thermodynamic urban surface temperature is represented by the surface temperatures of urban facets (roofs, roads, and walls), the causes of SUHIs based on them being yet to be thoroughly investigated. Here, we examine the causes of SUHIs using facet surface temperatures simulated by a UCM. For this, the simulated surface energy fluxes at individual facets are area-weighted averaged and analyzed (facet approach). Two-dimensional idealized simulations are conducted, roughly representing mid-latitude hot and dry summer conditions. In both approaches, the primary cause of daytime SUHI is less evapotranspiration in the urban area. The amount of net shortwave radiation averaged over facets (inside the urban conceptual volume) is smaller (larger) than that at the rural surface, being interpreted to weaken (intensify) the daytime SUHI in the facet (bulk) approach. The nighttime SUHI is attributed to larger urban heat storage in the bulk approach but the trapping of longwave radiation in the facet approach. This study suggests that the facet approach is physically more consistent than the bulk approach in investigating the causes of SUHIs.

1 Introduction

As urbanization continues worldwide, weather and climate modifications due to urbanization become increasingly evident (Masson et al. 2020). One of the most obvious weather and climate modifications due to urbanization is the urban heat island (UHI), urban areas exhibiting a higher temperature than their surrounding rural areas (Deilami et al. 2018). The UHI affects not only thermal environment in urban areas but also local winds and air quality (Sarrat et al. 2006; Han and Baik 2008; Heaviside et al. 2017). Because of its importance and impacts, the UHI is one of the foremost issues in urban climate research (Arnfield 2003).

There have been numerous efforts to better understand UHIs (Kanda 2007; Mills 2014). In particular, the developments of urban canopy models (UCMs) in recent decades have made it possible to better simulate and understand UHIs (Martilli 2007; Qian et al. 2022). UCMs simulate the physical processes that occur at urban surfaces more realistically than slab models (Garuma 2018). In UCMs, the urban surface is represented as roofs, roads, and walls (facets) that form urban canyons. For each facet, the surface temperature and surface energy fluxes that satisfy the surface energy balance are calculated using given meteorological conditions and thermal and morphological parameters. The surface energy balance equation for each facet (Oke et al. 2017) is expressed as follows:

$$\begin{aligned} &\mathrm{SW_{down}}^{*} + \mathrm{LW_{down}}^{*} = Q_{\mathrm{H}}{}^{*} + Q_{\mathrm{E}}{}^{*} + Q_{\mathrm{C}}{}^{*} \\ &+ \alpha^{*}\mathrm{SW_{down}}^{*} + (1-\varepsilon^{*})\mathrm{LW_{down}}^{*} + \mathrm{LW_{emit}}^{*} (= \varepsilon^{*}\sigma {T_{\mathrm{s}}}^{*4}) \end{aligned} \quad (1)$$

✉ Jong-Jin Baik
jjbaik@snu.ac.kr

✉ Han-Gyul Jin
hgjin@pusan.ac.kr

[1] School of Earth and Environmental Sciences, Seoul National University, Seoul 08826, South Korea

[2] Department of Atmospheric Sciences, Pusan National University, Busan 46241, South Korea

[3] Institute for Future Earth, Pusan National University, Busan 46241, South Korea

Published online: 01 August 2025

Here, the asterisk indicates the facet, SW_{down}^{*} and LW_{down}^{*} are, respectively, the downward shortwave radiation and downward longwave radiation at the facet, Q_H^{*}, Q_E^{*}, and Q_C^{*} are, respectively, the sensible heat flux, latent heat flux, and storage heat flux at the facet, α^{*} is the facet surface albedo, ε^{*} is the facet surface emissivity, LW_{emit} is the emitted longwave radiation from the facet surface, σ is the Stefan-Boltzmann constant, and T_s^{*} is the facet surface temperature. LW_{emit}^{*} is calculated as $\varepsilon^{*}\sigma T_s^{*4}$. Q_C^{*} refers to the conductive heat flux between the facet surface and the facet subsurface. Equation 1 states that the downward shortwave and longwave radiations at the facet are balanced by the sensible heat flux, latent heat flux, storage heat flux, reflected shortwave radiation, reflected longwave radiation, and emitted longwave radiation at the facet.

Next, to provide the lower boundary conditions for atmospheric models, UCMs calculate the energy fluxes that satisfy the energy balance for an urban conceptual volume which includes roads and buildings and extends from a below-ground depth to a level above the roof-top level (Grimmond et al. 2010). Neglecting the net horizontal advection of energy, the energy balance equation for the conceptual volume (Oke 1988) is given by

$$\begin{aligned} &SW_{down} + LW_{down} + Q_{AH} = Q_H + Q_E + Q_C \\ &+ \alpha SW_{down} + (1-\varepsilon)LW_{down} + LW_{emit}(= \varepsilon\sigma T_s^{4}) \end{aligned} \quad (2)$$

Here, SW_{down} and LW_{down} are, respectively, the downward shortwave radiation and downward longwave radiation at the top surface of the conceptual volume, Q_{AH} is the flux of anthropogenic heat emitted into the conceptual volume, Q_H and Q_E are, respectively, the sensible heat flux and latent heat flux at the top surface of the conceptual volume, Q_C is the storage heat flux for the conceptual volume, α is the system albedo of the conceptual volume, ε is the system emissivity of the conceptual volume, and T_s is the representative urban surface temperature for the conceptual volume. Note that Q_C refers to the net heat storage change of all urban fabrics. Equation 2 states that the downward shortwave and longwave radiations at the top surface of the conceptual volume and anthropogenic heat emitted into the conceptual volume are balanced by the sensible heat flux, latent heat flux, reflected shortwave radiation, reflected longwave radiation, and emitted longwave radiation at the top surface of the conceptual volume and heat storage change of all urban fabrics inside the conceptual volume. The surface energy balances taken into consideration in UCMs are schematically presented in Fig. 1.

Using UCMs online- or offline-coupled with atmospheric models, many studies have explored surface UHIs (SUHIs) and SUHI causes in various cities (e.g., Zhao et al. 2014; Cao et al. 2016; Zhao et al. 2018; Fitria et al. 2019; Li et al. 2019; Harmay et al. 2021; Li and Zhang 2021; Wang and Li 2021; Li et al. 2024). The SUHI refers to the UHI occurring at the surface (Stewart and Mills 2021) and arises from the different characteristics of urban and rural surface energy balances (Zhou et al. 2018; Shen et al. 2021). For example, Li et al. (2019) examined the contributions of biophysical factors to the SUHIs in cities of North America and showed that the daytime (nighttime) SUHI is mainly caused by less evapotranspiration (larger heat storage) in urban areas than in rural areas. Li and Zhang (2021) showed that the

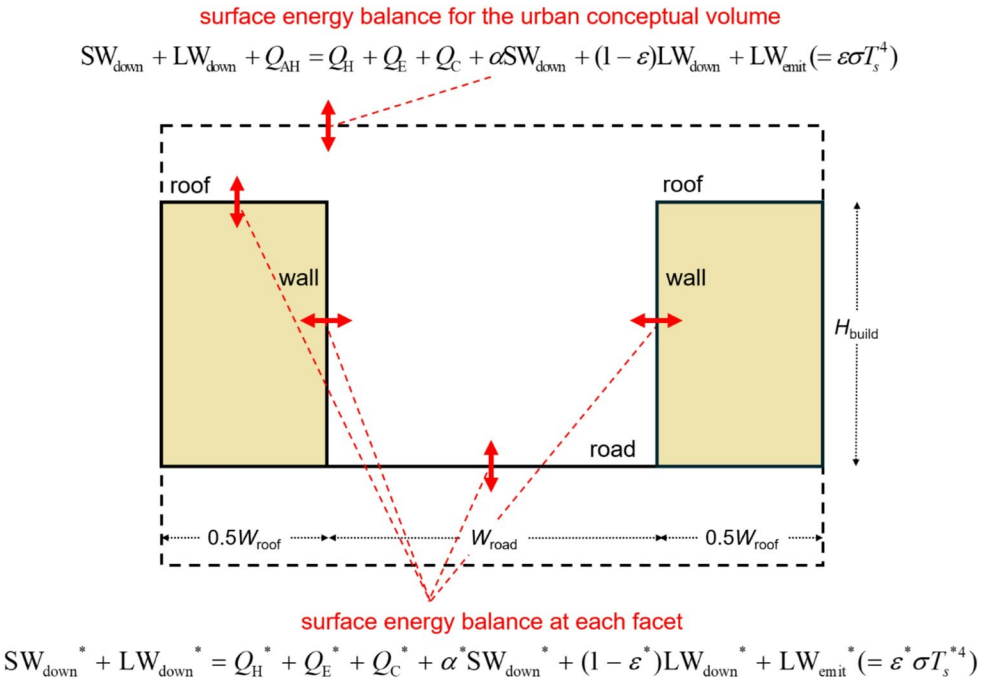

Fig. 1 Schematic diagram of the surface energy balances taken into consideration in urban canopy models. The dashed rectangle indicates the urban conceptual volume. W_{roof}, W_{road}, and H_{build} indicate the roof width, road width, and building height, respectively

less efficient sensible heat transfer from the surface to the adjacent air in urban areas is primarily responsible for the daytime SUHIs in cities within the southern region of East China in summer.

To find the causes of SUHIs, the previous studies of SUHIs employing UCMs used the surface energy fluxes which are balanced for the urban conceptual volume (Eq. 2) to characterize the urban surface energy balance and compared them with rural surface energy fluxes. This approach is called the bulk approach in this study. In this bulk approach, most of the urban surface energy fluxes including the emitted longwave radiation are represented at the top surface of the conceptual volume (Eq. 2). Accordingly, the representative urban surface temperature satisfying the energy balance for the conceptual volume (T_s in Eq. 2) is the radiative surface temperature which is inverted from the emitted longwave radiation at the top surface of the conceptual volume (LW_{emit}). Meanwhile, the thermodynamic urban surface temperature, which indicates the actual thermodynamic state of urban surface, is represented by the area-weighted average of surface temperatures of facets (Oke et al. 2017). It should be noted that this thermodynamic urban surface temperature is not the same as the radiative urban surface temperature due to the complex geometry of urban surface. Given that each facet's surface temperature satisfies Eq. 1, the energy fluxes corresponding to the thermodynamic urban surface temperature are the area-weighted averages of individual facets' energy fluxes. Comparing these energy fluxes with rural surface energy fluxes, called the facet approach in this study, can provide deeper insights into the causes of SUHIs, but this has not been attempted in previous studies of SUHIs using UCMs. This motivates the present study.

In this study, we examine the causes of SUHIs using facet surface temperatures and energy fluxes in the facet approach and present how the causes of SUHIs in the facet approach are different from those in the conventional approach, that is, the bulk approach. For this, the Weather Research and Forecasting (WRF) model that includes a UCM is utilized. In Section 2, the numerical model, experimental design, and analysis method are described. The results and discussion are given in Section 3. Section 4 gives a summary and conclusions.

2 Numerical model, experimental design, and analysis method

2.1 Numerical model and experimental design

Two-dimensional idealized numerical simulations are conducted using the WRF model version 4.1.3 (Skamarock et al. 2019). For urban canopy parameterization, the Seoul National University UCM (SNUUCM) is used (Ryu et al. 2011). The SNUUCM is a single-layer UCM in which each facet has a single representative surface temperature and simulates various energy transfer processes that take place at urban surfaces including the absorption, reflection, and trapping of radiation, heat and moisture exchanges by turbulence, and conductive heat transfer. The surface energy transfer processes in the non-built-up (natural) area are simulated by the unified Noah land surface model (Chen and Dudhia 2001). Table 1 provides other physics parameterization schemes used in the control experiment.

To examine whether the main causes of SUHIs found from the control experiment differ with changes in each of urban canopy, planetary boundary layer, and radiation parameterization schemes, sensitivity experiments are performed (Table 1). Most physics parameterization schemes adopted in the control and sensitivity experiments are among the most widely used schemes by researchers (https://www2.mmm.ucar.edu/wrf/users/physics/wrf_physics_survey.pdf). The urban-parameter values used in the control experiment are listed in Table 2. The thermal-parameter values adopted in the control experiment are within the range of those found for built materials (Oke et al. 2017) and were

Table 1 Physics parameterization schemes used in the control and sensitivity experiments

Physics parameterization	Control experiment	Sensitivity experiment
Urban surface physics	SNUUCM (Ryu et al. 2011)	SLUCM[a] (Kusaka et al. 2001)
Land surface physics	Unified Noah land surface model (Chen and Dudhia 2001)	same
Planetary boundary layer [surface layer]	Yonsei University [MM5] (Hong et al. 2006; Jiménez et al. 2012)	MYJ[b] [Eta[c]] (Janjić 1994)
Shortwave radiation	Dudhia (Dudhia 1989)	RRTMG_SW[d] (Iacono et al. 2008)
Longwave radiation	RRTM[e] (Mlawer et al. 1997)	RRTMG_LW[f] (Iacono et al. 2008)
Cloud microphysics	WRF single-moment 6-class (Hong and Lim 2006)	same

[a] single-layer UCM

[b] Mellor-Yamada-Janjić scheme

[c] Eta similarity scheme

[d] Rapid radiative transfer model for general circulation models_shortwave

[e] Rapid radiative transfer model

[f] Rapid radiative transfer model for general circulation models_longwave

Table 2 Values of urban parameters used in the control and sensitivity experiments

Urban parameter	Control experiment	Sensitivity experiment
Built-up/Natural area fraction	0.9/0.1	0.9/0.1
Roof width (m)	10	10
Mean building height (m)	10	10
Canyon orientation (°)	180	180
Canyon aspect ratio	1.0	1.5 ($CAR_{1.5}$), 0.5 ($CAR_{0.5}$)
Albedo of roof, road, and wall	0.18	0.27 ($ALB_{0.27}$), 0.09 ($ALB_{0.09}$)
Emissivity of roof, road, and wall	0.95	0.95
Heat capacity of roof, road, and wall (MJ m^{-3} K^{-1})	1.4	2.1 ($HC_{2.1}$), 0.7 ($HC_{0.7}$)
Thermal conductivity of roof, road, and wall (J m^{-1} s^{-1} K^{-1})	0.8	1.2 ($TC_{1.2}$), 0.4 ($TC_{0.4}$)
Daily maximum anthropogenic heat flux (W m^{-2})	0	90 (AH_{90})

used in previous modeling studies (e.g., Hamdi and Schayes 2008; Miao et al. 2009; Ryu and Baik 2012; Krayenhoff et al. 2014; Tsiringakis et al. 2020). The albedo (emissivity) of the rural surface is set as 0.18 (0.985). Additional sensitivity experiments are performed to examine whether the main causes of SUHIs found from the control experiment differ with changes in each urban-parameter value (Table 2). In the urban-parameter sensitivity experiments, the value of an urban morphological or thermal parameter is set to either 50% or 150% of that in the control experiment. The influence of including anthropogenic heat is also examined by conducting a sensitivity experiment in which a diurnally varying anthropogenic heat profile (Chen et al. 2011) with a maximum of 90 W m^{-2} is included.

Figure 2a illustrates the simulation domain configuration. The domain is two-dimensional with a horizontal (vertical) size of 200 (7) km. The Rayleigh damping is applied to the layer above 5 km (Klemp et al. 2008). The model horizontal resolution is 500 m. Vertically, the number of layers is 66, with 45 layers located below 2 km. An urban area with a horizontal size of 20 km whose center is situated at the domain center is considered. The rural land use type is cropland/woodland mosaic. The Coriolis force is neglected. Note that including the Coriolis effect has little influence on the SUHI intensity and main causes of SUHIs in each of the two approaches in our two-dimensional idealized simulations. As a lateral boundary condition, the periodic boundary condition is employed. A warm and dry (no clouds) summer condition in midlatitude (30°N) is considered (Fig. 2b and c). The slope of initial potential temperature profile is 5 K km^{-1}, the initial surface potential temperature being 298.15 K (Fig. 2b). The slope of initial water vapor mixing ratio profile is 0.33 g kg^{-1} km^{-1}, the initial surface water vapor mixing ratio being 3 g kg^{-1} (Fig. 2c). There is no initial background wind. This domain setting makes it possible to investigate the main causes of SUHIs in each

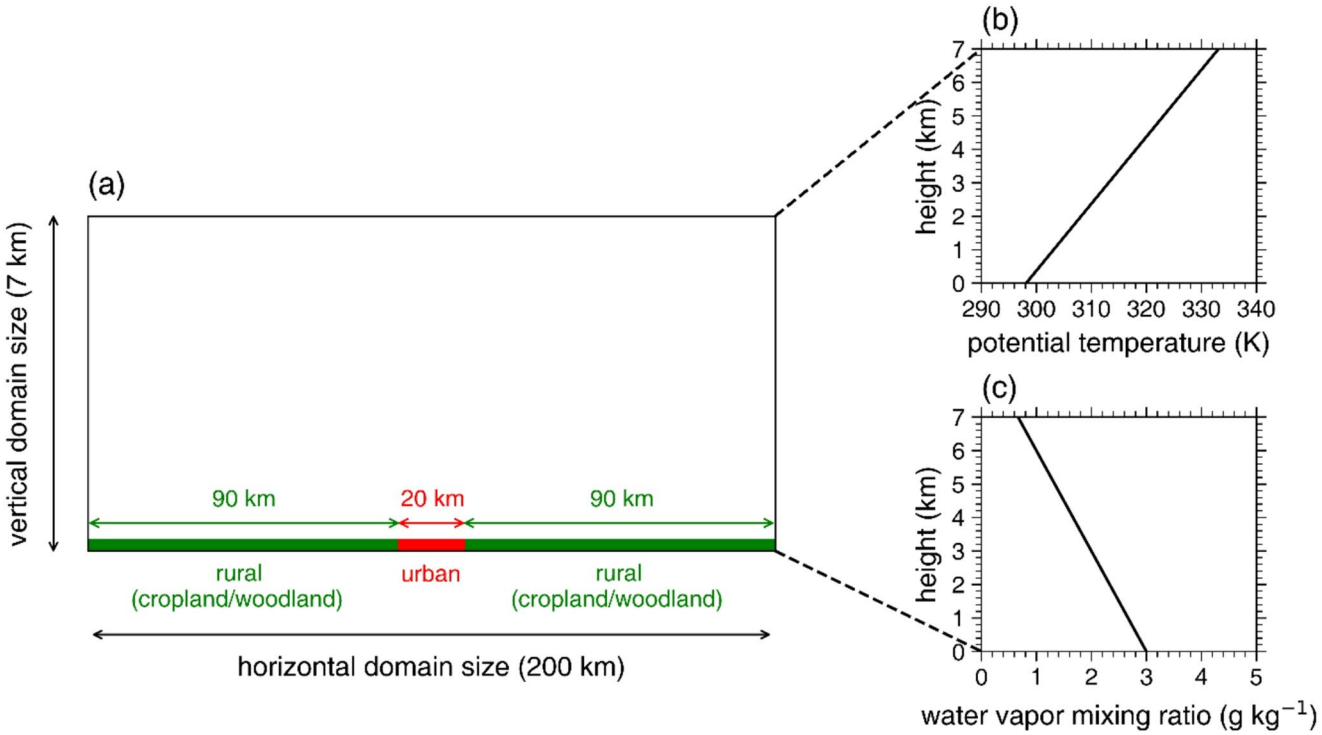

Fig. 2 (**a**) Domain configuration of numerical simulations and the vertical profiles of initial (**b**) potential temperature and (**c**) water vapor mixing ratio

of the two approaches in a simple urban-rural configuration without complicated synoptic and geographical influences.

To obtain more robust results, ensemble simulations are performed with 10 ensemble members for each experiment (Tabassum et al. 2024). To generate the ensemble members, the initial potential temperatures at the three lowest model levels are perturbed by adding random perturbations of potential temperature ranging from −0.1 K to 0.1 K (Hong et al. 2024). Starting from 0000 LST 21 June, the 53-h integration of the WRF model is performed with a time step of 2 s. For analysis, the data of the last 24-h integration are used.

2.2 Analysis method

2.2.1 Bulk approach

In the bulk approach, the urban surface energy fluxes in Eq. 2 are compared with rural surface energy fluxes to investigate the causes of SUHIs. Equation 2 can be re-written as follows:

$$\begin{aligned} &\mathrm{SW_{down}}(1-\alpha)+\varepsilon\mathrm{LW_{down}}+Q_{\mathrm{AH}}= \\ &Q_{\mathrm{H}}+Q_{\mathrm{E}}+Q_{\mathrm{C}}+\mathrm{LW_{emit}}(=\varepsilon\sigma {T_{\mathrm{s}}}^4) \end{aligned} \tag{3}$$

Note that each urban surface energy flux in Eq. 3 for an urban grid is the area-weighted average over the built-up area and natural area and is used for analysis:

$$E_{\mathrm{urban}}=f_{\text{built-up}}E_{\text{built-up}}+(1-f_{\text{built-up}})E_{\mathrm{natural}} \tag{4}$$

where E_{urban} is each urban surface energy flux in Eq. 3 ($\mathrm{SW_{down}}(1-\alpha)$, $\varepsilon\mathrm{LW_{down}}$, Q_{AH}, Q_{H}, Q_{E}, Q_{C}, and $\mathrm{LW_{emit}}$) for an urban grid, $f_{\text{built-up}}$ is the built-up area fraction, and $E_{\text{built-up}}$ and E_{natural} are the urban surface energy fluxes in Eq. 3 in the built-up and natural areas, respectively.

As mentioned in Section 1, in the bulk approach, the representative urban surface temperature satisfying the energy balance for the urban conceptual volume is the radiative surface temperature which is inverted from the emitted longwave radiation at the top surface of the conceptual volume. Thus, for an urban grid, the urban surface temperature in the bulk approach, $T_{\mathrm{s,u(bulk)}}$, is expressed as

$$T_{\mathrm{s,u(bulk)}}= \left[\frac{\mathrm{SW_{down}}(1-\alpha)+\varepsilon\mathrm{LW_{down}}+Q_{\mathrm{AH}}-Q_{\mathrm{H}}-Q_{\mathrm{E}}-Q_{\mathrm{C}}}{\varepsilon\sigma}\right]^{\frac{1}{4}} \tag{5}$$

The system emissivity of the urban conceptual volume (ε) is assumed to be 0.954 which is the area-weighted average of the facet emissivity and the rural surface emissivity. The SUHI intensity in the bulk approach, $\mathrm{SUHII_{bulk}}$, is quantified as the average of $T_{\mathrm{s,u(bulk)}}$ over the urban grids minus the average of rural surface temperature ($T_{\mathrm{s,r}}$) over the rural grids:

$$\mathrm{SUHII_{bulk}}=T_{\mathrm{s,u(bulk)}}-T_{\mathrm{s,r}} \tag{6}$$

$T_{\mathrm{s,u(bulk)}}$ and $T_{\mathrm{s,r}}$ in Eq. 6 are the averages over the urban and rural grids, respectively.

To investigate the causes of SUHIs, the differences between the urban surface energy fluxes in the bulk approach and rural surface energy fluxes are analyzed:

$$\begin{aligned} &\Delta\mathrm{SW_{down}}(1-\alpha)+\Delta\varepsilon\mathrm{LW_{down}}+\Delta Q_{\mathrm{AH}} \\ &-\Delta Q_{\mathrm{H}}-\Delta Q_{\mathrm{E}}-\Delta Q_{\mathrm{C}}=\Delta\mathrm{LW_{emit}}(=\Delta\varepsilon\sigma {T_{\mathrm{s}}}^4) \end{aligned} \tag{7}$$

In Eq. 7, ΔA, where A is $\mathrm{SW_{down}}(1-\alpha)$, $\varepsilon\mathrm{LW_{down}}$, Q_{AH}, Q_{H}, Q_{E}, Q_{C}, or $\varepsilon\sigma {T_{\mathrm{s}}}^4$, is the average of A over the urban grids minus the average of A over the rural grids. The above equation states that the urban-rural differences in radiative, anthropogenic, sensible, latent, and storage heat fluxes determine the urban-rural difference in emitted longwave radiation and therefore $\mathrm{SUHII_{bulk}}$. Note that ΔQ_{AH} is zero in the control experiment because no anthropogenic heat is applied.

2.2.2 Facet approach

In the facet approach, we use the complete urban surface temperature which is the area-weighted average of surface temperatures of all facets (roofs, roads, and walls) to represent the thermodynamic urban surface temperature (Voogt and Oke 1997). Accordingly, for an urban grid, the urban surface temperature in the facet approach, $T_{\mathrm{s,u(facet)}}$, is given by

$$\begin{aligned} &T_{\mathrm{s,u(facet)}}= \\ &f_{\text{built-up}}\frac{W_{\mathrm{roof}}T_{\mathrm{roof}}+W_{\mathrm{road}}T_{\mathrm{road}}+2H_{\mathrm{build}}T_{\mathrm{wall}}}{W_{\mathrm{roof}}+W_{\mathrm{road}}+2H_{\mathrm{build}}} \\ &+(1-f_{\text{built-up}})T_{\mathrm{s(natural)}} \end{aligned} \tag{8}$$

Here, W_{roof} is the roof width, W_{road} is the road width, H_{build} is the building height, T_{roof}, T_{road}, and T_{wall} are, respectively, the surface temperatures of roofs, roads, and walls, and $T_{\mathrm{s(natural)}}$ is the surface temperature of the natural area for the urban grid. The SUHI intensity in the facet approach, $\mathrm{SUHII_{facet}}$, is quantified as the average of $T_{\mathrm{s,u(facet)}}$ over the urban grids minus the average of $T_{\mathrm{s,r}}$ over the rural grids:

$$\mathrm{SUHII_{facet}}=T_{\mathrm{s,u(facet)}}-T_{\mathrm{s,r}} \tag{9}$$

$T_{\mathrm{s,u(facet)}}$ and $T_{\mathrm{s,r}}$ in Eq. 9 are the averages over the urban and rural grids, respectively. Note that $T_{\mathrm{s,r}}$ and rural surface

energy fluxes which are treated in the Noah land surface model are identical in both bulk and facet approaches.

In the facet approach, the urban surface energy fluxes in Eq. 1 are area-weighted averaged over facets and compared with rural surface energy fluxes to investigate the causes of SUHIs. Equation 1 can be re-written as follows:

$$\mathrm{SW_{down}}^*(1-\alpha^*)+\varepsilon^*\mathrm{LW_{down}}^* = Q_\mathrm{H}^*+Q_\mathrm{E}^*+Q_\mathrm{C}^*+\mathrm{LW_{emit}}^*(=\varepsilon^*\sigma {T_\mathrm{s}}^{*4}) \quad (10)$$

Corresponding to the definition of $T_{\mathrm{s,u(facet)}}$, each urban surface energy flux in Eq. 10 for an urban grid is obtained by taking the area-weighted average in the same way as in Eq. 8 and is used for analysis:

$$E_\mathrm{urban}{}^* = f_\mathrm{built\text{-}up}\frac{W_\mathrm{roof}E_\mathrm{roof}{}^*+W_\mathrm{road}E_\mathrm{road}{}^*+2H_\mathrm{build}E_\mathrm{wall}{}^*}{W_\mathrm{roof}+W_\mathrm{road}+2H_\mathrm{build}} + (1-f_\mathrm{built\text{-}up})E_\mathrm{natural}{}^* \quad (11)$$

Here, $E_\mathrm{urban}{}^*$ is each urban surface energy flux in Eq. 10 ($\mathrm{SW_{down}}^*(1-\alpha^*)$, $\varepsilon^*\mathrm{LW_{down}}^*$, Q_H^*, Q_E^*, Q_C^*, and $\mathrm{LW_{emit}}^*$) for an urban grid, $E_\mathrm{roof}{}^*$, $E_\mathrm{road}{}^*$, and $E_\mathrm{wall}{}^*$ are, respectively, the urban surface energy fluxes in Eq. 10 at roofs, roads, and walls, and $E_\mathrm{natural}{}^*$ is the urban surface energy flux in Eq. 10 in the natural area.

The differences between urban surface energy fluxes in the facet approach and rural surface energy fluxes are analyzed to investigate the causes of SUHIs:

$$\Delta\mathrm{SW_{down}}^*(1-\alpha^*)+\Delta\varepsilon^*\mathrm{LW_{down}}^* - \Delta Q_\mathrm{H}^*-\Delta Q_\mathrm{E}^*-\Delta Q_\mathrm{C}^*=\Delta\mathrm{LW_{emit}}^*(=\Delta\varepsilon^*\sigma {T_\mathrm{s}}^{*4}) \quad (12)$$

In the above equation, $\Delta\mathrm{A}^*$, where A^* is $\mathrm{SW_{down}}^*(1-\alpha^*)$, $\varepsilon^*\mathrm{LW_{down}}^*$, Q_H^*, Q_E^*, Q_C^*, or $\varepsilon^*\sigma {T_\mathrm{s}}^{*4}$, is the average of A^* over the urban grids minus the average of A^* over the rural grids. As in Eq. 7, the above equation states that the urban-rural differences in radiative, sensible, latent, and storage heat fluxes determine the urban-rural difference in emitted longwave radiation and therefore $\mathrm{SUHII_{facet}}$. The main analysis of the causes of SUHIs in both approaches is made for the daytime and nighttime which are defined as the period over 1200–1700 LST and that over 0000–0500 LST, respectively (Ryu and Baik 2012).

3 Results and discussion

3.1 SUHI intensity

The diurnal variations of $T_{\mathrm{s,u(facet)}}$, $T_{\mathrm{s,u(bulk)}}$, and $T_{\mathrm{s,r}}$ in the control experiment are shown in Fig. 3a. Both $T_{\mathrm{s,u(facet)}}$ and $T_{\mathrm{s,u(bulk)}}$ in the control experiment fall within the range of urban surface temperatures observed in many mid-latitude cities during summer (e.g., Song and Park 2014; Feng et al. 2020; Chang et al. 2021; Shi et al. 2022). From 0510 LST, shortly after sunrise, to 0750 LST, both $T_{\mathrm{s,u(facet)}}$ and $T_{\mathrm{s,u(bulk)}}$ increase more gradually than $T_{\mathrm{s,r}}$. On the other hand, during 0810–1300 LST, both $T_{\mathrm{s,u(facet)}}$ and $T_{\mathrm{s,u(bulk)}}$ increase more rapidly than $T_{\mathrm{s,r}}$. During the daytime (1200–1700 LST), $T_{\mathrm{s,u(facet)}}$ and $T_{\mathrm{s,u(bulk)}}$ peak, respectively, 40 and 10 min later and exhibit much larger maximum values than $T_{\mathrm{s,r}}$. After 1800 LST, about one hour before sunset, $T_{\mathrm{s,u(facet)}}$ and $T_{\mathrm{s,u(bulk)}}$ exhibit more gradual declines than $T_{\mathrm{s,r}}$. It is noticeable that $T_{\mathrm{s,u(facet)}}$ is lower than $T_{\mathrm{s,u(bulk)}}$ during 0700–1440 LST, that is, the complete urban surface temperature is lower than the radiative urban surface temperature during this period. The maximum $T_{\mathrm{s,u(facet)}}$ is lower than the maximum $T_{\mathrm{s,u(bulk)}}$ by 1.40 °C, and the daytime mean $T_{\mathrm{s,u(facet)}}$ and $T_{\mathrm{s,u(bulk)}}$ are 46.5 and 46.9 °C, respectively. During the nighttime (0000–0500 LST), $T_{\mathrm{s,u(facet)}}$ is slightly higher than $T_{\mathrm{s,u(bulk)}}$, the mean difference between $T_{\mathrm{s,u(facet)}}$ and $T_{\mathrm{s,u(bulk)}}$ being 1.00 °C. The difference between $T_{\mathrm{s,u(facet)}}$ and $T_{\mathrm{s,u(bulk)}}$ increases when a higher canyon aspect ratio is considered. The canyon aspect ratio is defined as $H_\mathrm{build}/W_\mathrm{road}$. In the $\mathrm{CAR_{1.5}}$ experiment in which the canyon aspect ratio (CAR) is increased to 1.5 by reducing W_road to two-thirds of its value in the control experiment, the mean difference between $T_{\mathrm{s,u(facet)}}$ and $T_{\mathrm{s,u(bulk)}}$ is

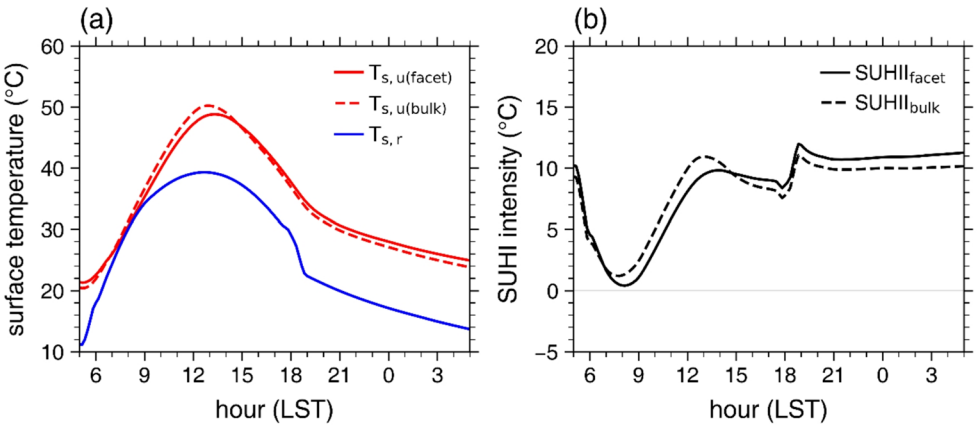

Fig. 3 (**a**) Diurnal variations of urban surface temperature in the facet approach (complete urban surface temperature) (red solid line), urban surface temperature in the bulk approach (radiative urban surface temperature) (red dashed line), and rural surface temperature (blue solid line) in the control experiment. (**b**) Diurnal variations of surface urban heat island intensities in the facet approach (black solid line) and bulk approach (black dashed line) in the control experiment

larger than that in the control experiment by 1.04 °C during the daytime and by 0.29 °C during the nighttime.

Figure 3b shows the diurnal variations of $SUHII_{facet}$ and $SUHII_{bulk}$ in the control experiment. Despite somewhat differences in $SUHII_{facet}$ and $SUHII_{bulk}$, their diurnal variations are qualitatively similar. $SUHII_{facet}$ and $SUHII_{bulk}$ are weakest at 0810 and 0750 LST, being 0.40 and 1.19 °C, respectively. During the daytime, $SUHII_{facet}$ ($SUHII_{bulk}$) peaks at 1350 (1300) LST and the mean $SUHII_{facet}$ ($SUHII_{bulk}$) is 9.31 (9.70) °C. During the nighttime, both $SUHII_{facet}$ and $SUHII_{bulk}$ exhibit slight variations and the mean $SUHII_{facet}$ (11.03 °C) is higher than the mean $SUHII_{bulk}$ (10.03 °C) by 1.00 °C. The diurnal variation of $SUHII_{facet}$ is qualitatively consistent with the typical diurnal variation of SUHI intensity defined using the complete urban surface temperature (Oke et al. 2017). Meanwhile, Stewart et al. (2021) investigated the diurnal variations of SUHI intensities in cities under various background climates using the temperatures of plan-view horizontal urban surfaces (roofs and roads). They showed that the diurnal variation of SUHI intensity defined using the temperatures of plan-view horizontal urban surfaces in subtropical cities surrounded by vegetated rural surfaces exhibits an inverse spoon pattern (Lai et al. 2018) in which the SUHI intensity is stronger during the daytime than during the nighttime. We calculated the SUHI intensity for which the built-up surface temperature is defined as the area-weighted average of surface temperatures of roofs and roads. The calculated daytime (nighttime) mean SUHI intensity is 12.57 (8.99) °C, the diurnal variation of SUHI intensity exhibiting an inverse spoon pattern.

3.2 Comparisons between urban surface energy fluxes in the bulk and facet approaches

In this subsection, how the urban surface energy fluxes in the bulk approach (Eq. 3) and those in the facet approach (Eq. 10) are different is analyzed. Figure 4 shows the diurnal variations of urban surface energy fluxes in the bulk approach ($SW_{down}(1-\alpha)$, εLW_{down}, Q_H, Q_E, and Q_C) in the control experiment along with those of rural surface energy fluxes. In the bulk approach, the urban $SW_{down}(1-\alpha)$ and εLW_{down} mean the amounts of shortwave and longwave radiations absorbed within the urban conceptual volume, respectively. During the daytime, the urban $SW_{down}(1-\alpha)$ is slightly larger than the rural $SW_{down}(1-\alpha)$ (Fig. 4a). This is because the multiple reflections occurring within the urban canyon cause the system albedo of the urban conceptual volume to be lower than the albedo of the rural surface (Fortuniak 2008; Sugawara and Takamura 2014; Yang and Li 2015). The urban εLW_{down} is slightly smaller than the rural εLW_{down} during the daytime but is slightly larger during the nighttime (Fig. 4b). LW_{down}, the downward longwave radiation from the sky that passes through the top surface of the conceptual volume, is slightly larger in the urban area than

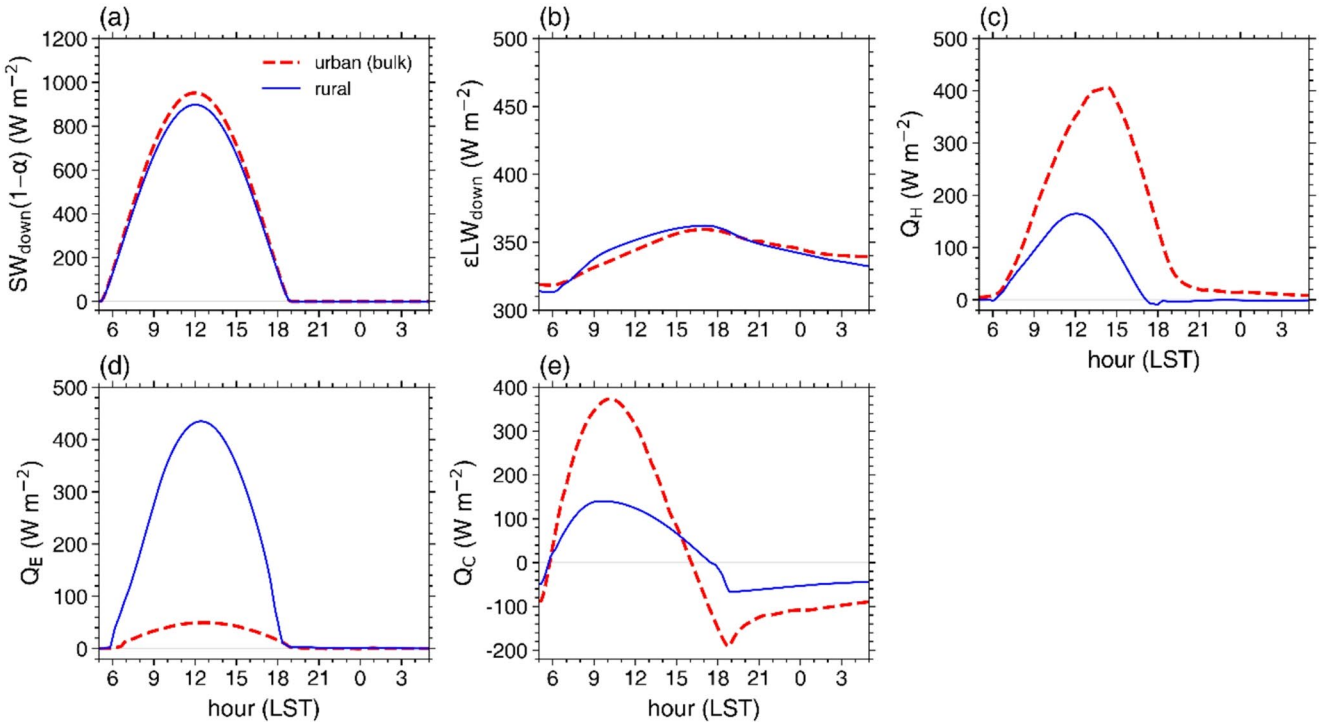

Fig. 4 Diurnal variations of urban (**a**) net shortwave radiation ($SW_{down}(1-\alpha)$), (**b**) absorbed longwave radiation (εLW_{down}), (**c**) sensible heat flux (Q_H), (**d**) latent heat flux (Q_E), and (**e**) storage heat flux (Q_C) in the bulk approach (red dashed line) in the control experiment. The blue solid lines indicate the rural surface energy fluxes

in the rural area throughout the day, while ε of the urban conceptual volume is smaller than ε of the rural surface.

The urban Q_H and Q_E in the bulk approach mean the sensible and latent heat fluxes through the top surface of the urban conceptual volume, respectively. The urban Q_H is overall much larger than the rural Q_H (Fig. 4c), whereas the urban Q_E is overall much smaller than the rural Q_E (Fig. 4d). These results were also found in many previous studies (e.g., Chen et al. 2014; Wang and Li 2021). The daytime mean urban (rural) Q_H is 356.7 (103.3) W m^{-2}, and the daytime mean urban (rural) Q_E is 42.6 (355.8) W m^{-2}. The urban Q_C in the bulk approach means the net heat storage change of all urban fabrics inside the urban conceptual volume. Throughout the day, the urban Q_C generally exhibits much larger magnitudes than the rural Q_C (Fig. 4e). The larger heat storage in urban areas than in rural areas was reported in many previous studies (e.g., Wang et al. 2020; Chew et al. 2021). The daytime mean urban (rural) Q_C is 123.2 (75.1) W m^{-2}, and the nighttime mean urban (rural) Q_C is −99.9 (−47.8) W m^{-2}.

Figure 5 shows the diurnal variations of urban surface energy fluxes in the facet approach ($SW_{down}^*(1-\alpha^*)$, $\varepsilon^* LW_{down}^*$, Q_H^*, Q_E^*, and Q_C^*) in the control experiment along with those of rural surface energy fluxes. Note that the rural surface energy fluxes are identical in the bulk and facet approaches. In the facet approach, the urban $SW_{down}^*(1-\alpha^*)$ and $\varepsilon^* LW_{down}^*$ indicate the mean amounts of shortwave and longwave radiations absorbed by individual facets, respectively. Contrary to the urban $SW_{down}(1-\alpha)$ in the bulk approach, the urban $SW_{down}^*(1-\alpha^*)$ in the facet approach is considerably smaller than the rural $SW_{down}^*(1-\alpha^*)$ (Fig. 5a). This is explained by the fact that the shade within the urban canyon causes the mean amount of shortwave radiation absorbed by individual facets to be smaller than that absorbed by the rural surface (Theeuwes et al. 2014; Saher et al. 2021). The urban $\varepsilon^* LW_{down}^*$ in the facet approach is much larger than the rural $\varepsilon^* LW_{down}^*$ (Fig. 5b), which is in contrast with the urban εLW_{down} in the bulk approach. This is because the urban $\varepsilon^* LW_{down}^*$ in the facet approach includes the trapped longwave radiation within the urban canyon as well as the longwave radiation which comes from the sky.

The urban Q_H^* and Q_E^* in the facet approach indicate the mean sensible and latent heat flux through individual facet surfaces. Despite the considerably smaller urban $SW_{down}^*(1-\alpha^*)$ (Fig. 5a), the urban Q_H^* is generally larger than the rural Q_H^* throughout the day (Fig. 5c), the urban-rural difference being smaller than that in the bulk approach. This indicates that the absorbed all-wave radiation ($SW_{down}^*(1-\alpha^*) + \varepsilon^* LW_{down}^*$) is more efficiently partitioned into the sensible heat flux at the facet surface than at the rural surface, in line with Ramamurthy et al. (2014). Consistent with the urban Q_E in the bulk approach, the urban Q_E^* in the facet approach is generally much smaller than the rural Q_E^*

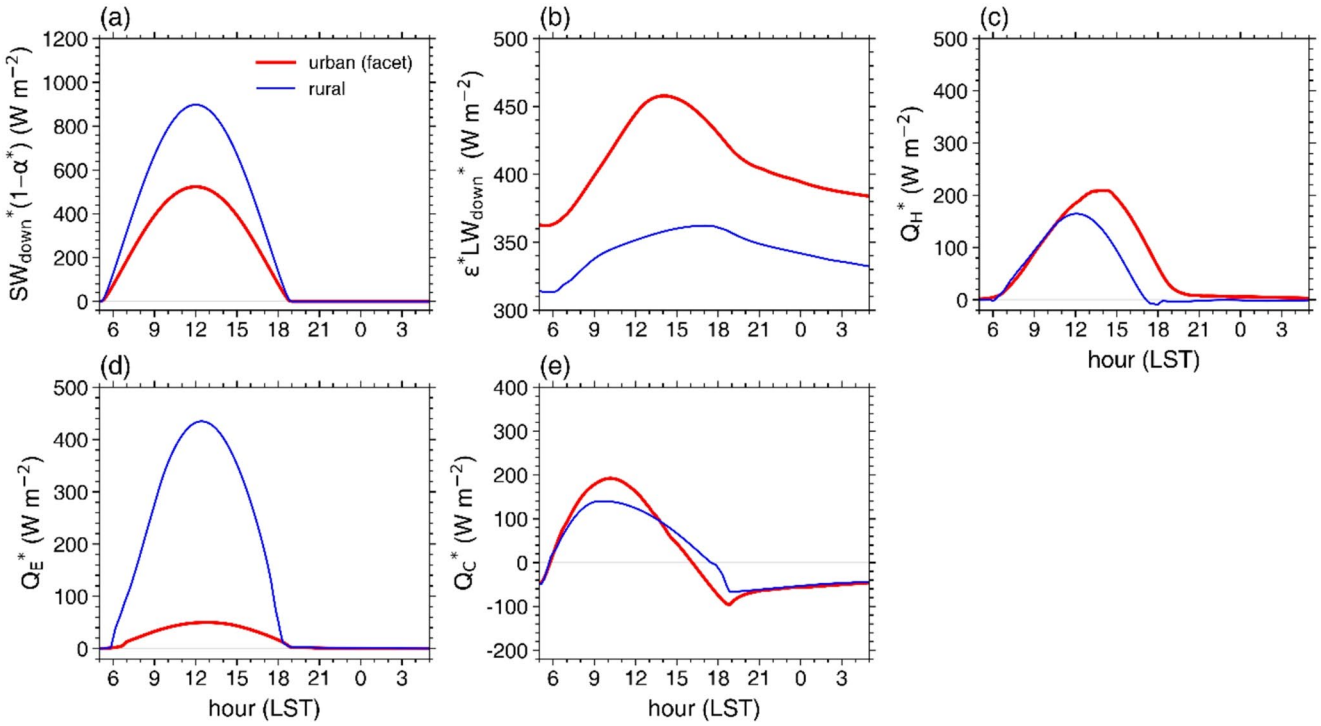

Fig. 5 Diurnal variations of urban (**a**) net shortwave radiation ($SW_{down}^*(1-\alpha^*)$), (**b**) absorbed longwave radiation ($\varepsilon^* LW_{down}^*$), (**c**) sensible heat flux (Q_H^*), (**d**) latent heat flux (Q_E^*), and (**e**) storage heat flux (Q_C^*) in the facet approach (red solid line) in the control experiment. The blue solid lines indicate the rural surface energy fluxes

(Fig. 5d). Since the latent heat fluxes at the facet surfaces are nearly zero, the urban latent heat fluxes in the bulk and facet approaches are very similar to each other. The mean urban Q_H^* (Q_E^*) is 183.1 (43.2) W m^{-2} during the daytime and 4.6 (0.2) W m^{-2} during the nighttime. The urban Q_C^* in the facet approach indicates the mean storage heat flux at individual facet surfaces. Unlike the urban Q_C in the bulk approach, the urban Q_C^* in the facet approach is slightly larger than the rural Q_C^* only during 0610–1340 LST and exhibits very small differences from the rural Q_C^* during the nighttime (Fig. 5e). This means that the amount of heat stored into all urban fabrics inside the urban conceptual volume is larger than the amount of heat stored into the rural subsurface but the amount of heat stored into individual facet subsurfaces does not significantly differ from that into the rural subsurface. Despite the relatively high thermal conductivity of the facets, the small differences between the urban Q_C^* and rural Q_C^* are to some extent because of the considerably smaller urban $SW_{down}^*(1-\alpha^*)$ than the rural $SW_{down}^*(1-\alpha^*)$ (Fig. 5a). The mean urban Q_C^* is 64.3 W m^{-2} during the daytime and −51.3 W m^{-2} during the nighttime.

Figures 4 and 5 reveal that the meaning of each urban surface energy flux significantly differs depending on how the urban surface energy balance is represented using the simulated energy fluxes by a UCM, which can lead the causes of SUHIs to be different. The causes of SUHIs in each of bulk and facet approaches are examined and compared with each other in the next subsection.

Figure 6 shows the diurnal variations of urban LW_{emit} in the bulk approach and urban LW_{emit}^* in the facet approach in the control experiment. The urban LW_{emit} in the bulk approach means the emitted longwave radiation through the top surface of the conceptual volume, while the urban LW_{emit}^* in the facet approach indicates the mean amount of longwave radiation emitted by individual facets. Consistent with the discrepancies between $T_{s,u(facet)}$ and $T_{s,u(bulk)}$ in Fig. 3a, the urban LW_{emit}^* in the facet approach is overall smaller (larger) than the urban LW_{emit} in the bulk approach during the daytime (nighttime). The mean difference between urban LW_{emit} in the bulk approach and urban LW_{emit}^* in the facet approach is 4.8 W m^{-2} during the daytime and is 5.7 W m^{-2} during the nighttime. The diurnal variation of $\varepsilon^*\sigma T_{s,\,u(facet)}^4$ is also plotted in Fig. 6 and is compared with those of urban LW_{emit} in the bulk approach and urban LW_{emit}^* in the facet approach. Overall, the urban LW_{emit}^* in the facet approach exhibits relatively small differences (<6.1 W m^{-2}) from $\varepsilon^*\sigma T_{s,\,u(facet)}^4$ during both daytime and nighttime. These slight differences are due to the heterogeneity of facet surface temperatures which makes the mean amount of emitted longwave radiation from individual facets (LW_{emit}^*) and $\varepsilon^*\sigma T_{s,\,u(facet)}^4$ slightly different. Meanwhile, the urban LW_{emit} in the bulk approach overall exhibits larger differences (up to 15.5 W m^{-2}) from $\varepsilon^*\sigma T_{s,\,u(facet)}^4$ than the urban LW_{emit}^* in the facet approach throughout the day. Thus, these results indicate that the surface energy fluxes in the facet approach ($SW_{down}^*(1-\alpha^*)$, $\varepsilon^*LW_{down}^*$, Q_H^*, Q_E^*, Q_C^*, and LW_{emit}^*;

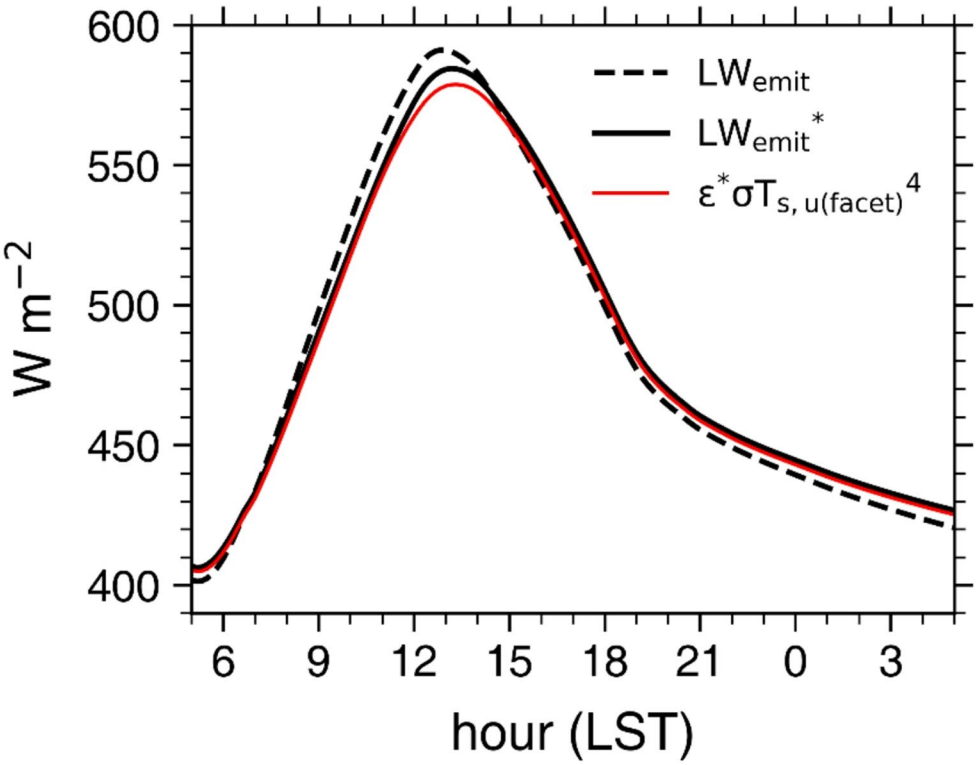

Fig. 6 Diurnal variations of urban emitted longwave radiations in the bulk approach (LW_{emit}, black dashed line) and in the facet approach (LW_{emit}^*, black solid line) and $\varepsilon^*\sigma T_{s,\,u(facet)}^4$ (red solid line) in the control experiment

Eq. 10) better correspond to the thermodynamic urban surface temperature (facet surface temperatures) than those in the bulk approach ($SW_{down}(1-\alpha)$, εLW_{down}, Q_H, Q_E, Q_C, and LW_{emit}; Eq. 3).

3.3 Causes of SUHIs in the bulk and facet approaches

Figure 7a shows the daytime and nighttime mean differences between urban surface energy fluxes in the bulk approach ($\Delta SW_{down}(1-\alpha)$, $\Delta\varepsilon LW_{down}$, $-\Delta Q_H$, $-\Delta Q_E$, and $-\Delta Q_C$) and rural surface energy fluxes in the control experiment. During the daytime, the mean $\Delta SW_{in}(1-\alpha)$ is 43.7 W m^{-2}, being interpreted as a factor intensifying the daytime SUHI. The mean $\Delta\varepsilon LW_{down}$ is very small during both daytime and nighttime. The daytime mean $-\Delta Q_H$ is −253.4 W m^{-2}, the greater sensible heat emission through the top surface of the urban conceptual volume being interpreted as a factor weakening the daytime SUHI. The most predominant urban-rural difference appears for $-\Delta Q_E$, the daytime mean $-\Delta Q_E$ being 313.1 W m^{-2}. Therefore, in the bulk approach, the less evapotranspiration in the urban area is the primary cause of the daytime SUHI. Many previous studies provided the same result (e.g., Taha 1997; Imhoff et al. 2010; Li et al. 2019). The daytime mean $-\Delta Q_C$ is −48.0 W m^{-2}, the greater heat storing into the urban fabrics inside the urban conceptual volume being interpreted as a factor weakening the daytime SUHI. During the nighttime, the predominant urban-rural difference appears for $-\Delta Q_C$, the nighttime mean $-\Delta Q_C$ being 52.1 W m^{-2}. The magnitudes of $\Delta\varepsilon LW_{down}$, $-\Delta Q_H$, and $-\Delta Q_E$ are very small (< 15 W m^{-2} in magnitude) and $\Delta SW_{down}(1-\alpha)$ is zero during the nighttime. These results indicate that in the bulk approach, the larger heat storage inside the urban conceptual volume is the primary cause of the nighttime SUHI. This agrees with many previous studies (e.g., Cao et al. 2016; Fitria et al. 2019; Li et al. 2019; Wang and Li 2021).

Figure 7b shows the daytime and nighttime mean differences between urban surface energy fluxes in the facet approach ($\Delta SW_{down}^*(1-\alpha^*)$, $\Delta\varepsilon^* LW_{down}^*$, $-\Delta Q_H^*$, $-\Delta Q_E^*$, and $-\Delta Q_C^*$) and rural surface energy fluxes in the control experiment. During the daytime, the mean $\Delta SW_{down}^*(1-\alpha^*)$ is −287.8 W m^{-2}, which is opposite in its sign to $\Delta SW_{down}(1-\alpha)$ in the bulk approach. Therefore, in the facet approach, $\Delta SW_{down}^*(1-\alpha^*)$ is interpreted as a factor predominantly weakening the daytime SUHI. The daytime

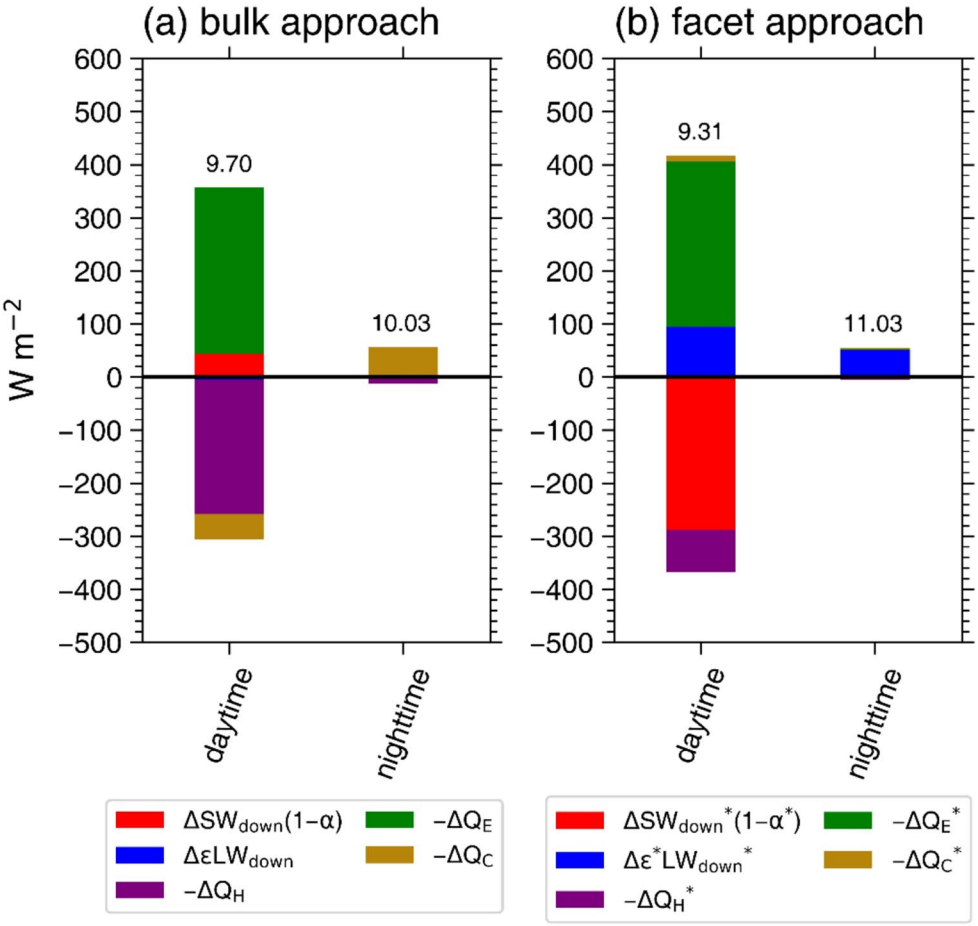

Fig. 7 (**a**) Stacked bar chart of daytime and nighttime mean differences between urban surface energy fluxes in the bulk approach and rural surface energy fluxes (urban minus rural) in the control experiment. The number above each bar indicates the surface urban heat island intensity in °C in the bulk approach. (**b**) Same as (a) except for the facet approach. The differences in net shortwave radiation, absorbed longwave radiation, sensible heat flux, latent heat flux, and storage heat flux are indicated by the red, blue, purple, green, and dark golden bars, respectively

mean $\Delta\varepsilon^{*}LW_{down}^{*}$ is 94.0 W m^{-2}, resulting from the trapping of longwave radiation. Accordingly, unlike $\Delta\varepsilon LW_{down}$ in the bulk approach, $\Delta\varepsilon^{*}LW_{down}^{*}$ in the facet approach is interpreted as a factor intensifying the daytime SUHI. The daytime mean $-\Delta Q_H^{*}$, $-\Delta Q_E^{*}$, and $-\Delta Q_C^{*}$ are −79.8, 312.6, and 10.8 W m^{-2}, respectively. These results reveal that the primary cause of the daytime SUHI in the facet approach is also the less evapotranspiration in the urban area. During the nighttime, the predominant urban-rural difference appears for $\Delta\varepsilon^{*}LW_{down}^{*}$, the nighttime mean $\Delta\varepsilon^{*}LW_{down}^{*}$ being 51.6 W m^{-2}. The magnitudes of $-\Delta Q_H^{*}$, $-\Delta Q_E^{*}$, and $-\Delta Q_C^{*}$ are very small (<10 W m^{-2} in magnitude), and $\Delta SW_{down}^{*}(1-\alpha^{*})$ is zero during the nighttime. These results indicate that in the facet approach, the greater absorption of longwave radiation at the facet surface than at the rural surface, which results from the trapping of longwave radiation, is the primary cause of the nighttime SUHI. It is found that the primary cause of the nighttime SUHI in the facet approach is different from that in the bulk approach.

Figure 7 reveals that the causes of SUHIs can differ depending on how the urban surface energy balance is represented using the simulated energy fluxes by a UCM. Given that the represented urban surface energy fluxes in the facet approach better correspond to the thermodynamic urban surface temperature than those in the bulk approach (Fig. 6), we suggest that the facet approach is physically more consistent framework than the bulk approach in examining the reason why the urban physical surfaces (facets) are warmer than the rural surfaces, that is the causes of SUHIs.

3.4 Sensitivity experiments

In this subsection, we examine whether the main findings on the causes of SUHIs in the bulk and facet approaches in the control experiment are robust in simulations with different physics parameterization schemes (Table 1) and urban-parameter values (Table 2). Figure 8 is the same as Fig. 7 except for the sensitivity experiments in which different physics parameterization schemes are used. Compared with the control experiment, changes in physics parameterization schemes lead to somewhat different $SUHII_{bulk}$ and $SUHII_{facet}$ during the daytime and nighttime. In the SLUCM experiment, both $SUHII_{bulk}$ and $SUHII_{facet}$ are stronger than in the control experiment during the daytime and nighttime. In

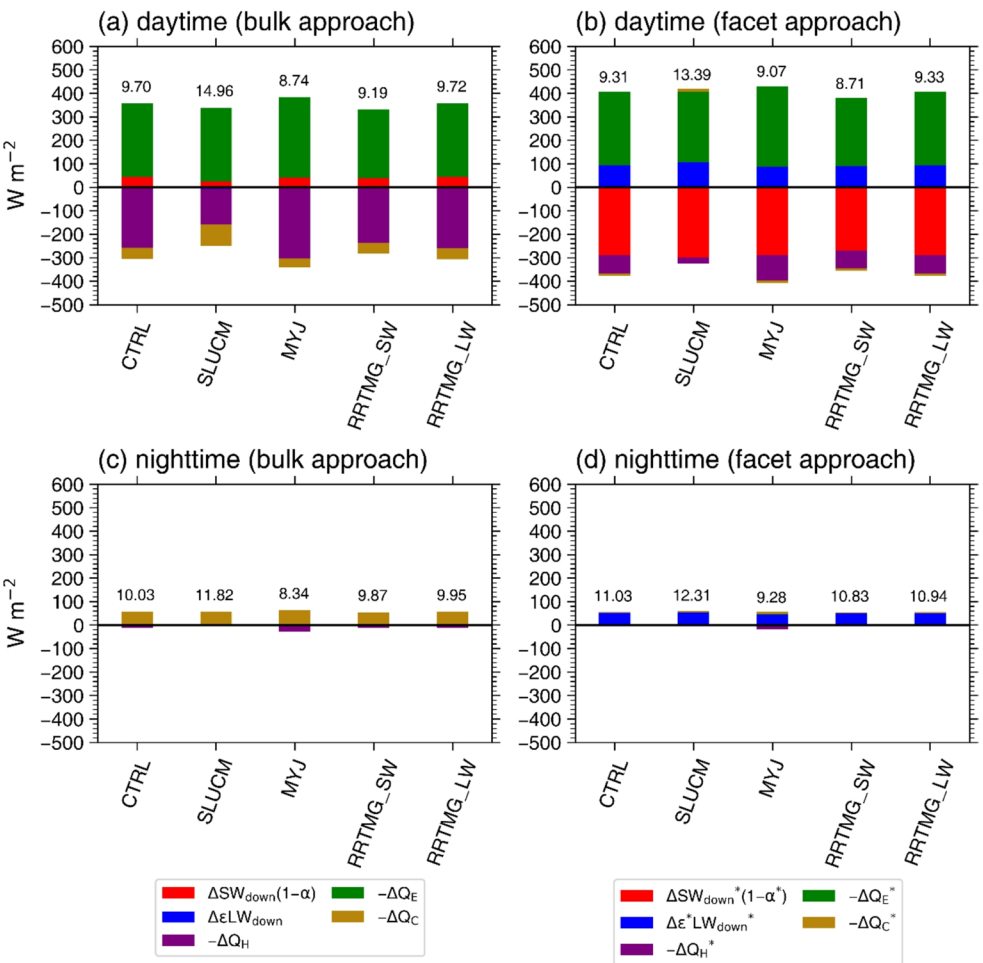

Fig. 8 (**a**, **c**) Same as Fig. 7a except for the sensitivity experiments of SLUCM, MYJ, RRTMG_SW, and RRTMG_LW. (**b**, **d**) Same as Fig. 7b except for the sensitivity experiments of SLUCM, MYJ, RRTMG_SW, and RRTMG_LW

both bulk and facet approaches, the most noticeable change responsible for the stronger daytime and nighttime SUHIs in the SLUCM experiment appears in the urban-rural difference in sensible heat flux. In the SLUCM experiment, the magnitude of daytime mean $-\Delta Q_H$ is smaller by 102.5 W m^{-2} and that of daytime mean $-\Delta Q_H^*$ is smaller by 51.9 W m^{-2} than in the control experiment. On the other hand, in the MYJ experiment, both $SUHII_{bulk}$ and $SUHII_{facet}$ are weaker than in the control experiment during the daytime and nighttime. In both bulk and facet approaches, the most noticeable change responsible for the weaker daytime and nighttime SUHIs in the MYJ experiment also appears in the urban-rural difference in sensible heat flux. In the MYJ experiment, the magnitude of daytime mean $-\Delta Q_H$ is larger by 49.6 W m^{-2} and that of daytime mean $-\Delta Q_H^*$ is larger by 26.7 W m^{-2} than in the control experiment. In the RRTMG_SW experiment, the daytime (nighttime) mean $SUHII_{bulk}$ is weaker by 0.51 (0.17) °C and the daytime (nighttime) mean $SUHII_{facet}$ is weaker by 0.60 (0.20) °C than in the control experiment. The differences in both $SUHII_{bulk}$ and $SUHII_{facet}$ between the RRTMG_LW experiment and the control experiment are very small during the daytime and nighttime. Figure 8 indicates that despite some variations of $SUHII_{bulk}$ and $SUHII_{facet}$ depending on physics parameterization schemes, the main causes of SUHIs in each of bulk and facet approaches are the same as those in the control experiment.

Figure 9 is the same as Fig. 7 except for the sensitivity experiments with different values of urban parameters. The change in canyon aspect ratio leads to noticeable changes in both $SUHII_{bulk}$ and $SUHII_{facet}$ during the daytime and nighttime. Compared with the $CAR_{0.5}$ experiment, in the $CAR_{1.5}$ experiment, the daytime mean $SUHII_{bulk}$ ($SUHII_{facet}$) is weaker by 4.11 (5.33) °C but the nighttime mean $SUHII_{bulk}$ ($SUHII_{facet}$) is stronger by 1.23 (1.99) °C. With increasing canyon aspect ratio, in the bulk approach, the magnitudes of the daytime $-\Delta Q_H$ and nighttime $-\Delta Q_C$ prominently increase, resulting in the decrease in daytime $SUHII_{bulk}$ and the increase in nighttime $SUHII_{bulk}$, respectively. Meanwhile, in the facet approach, the increase in canyon aspect ratio prominently increases the magnitudes of the daytime $\Delta SW_{down}^*(1-\alpha^*)$ and nighttime $\Delta\varepsilon^* LW_{down}^*$, resulting in the decrease in daytime $SUHII_{facet}$ and the increase in nighttime $SUHII_{facet}$, respectively. Increasing the albedo of urban facets leads to decreases in both $SUHII_{bulk}$ and $SUHII_{facet}$ during the daytime and nighttime. Compared with the $ALB_{0.09}$ experiment, in the $ALB_{0.27}$ experiment, the daytime mean $SUHII_{bulk}$ ($SUHII_{facet}$) is weaker by 1.91 (1.70) °C and the nighttime mean $SUHII_{bulk}$ ($SUHII_{facet}$) is weaker by 0.62 (0.57) °C.

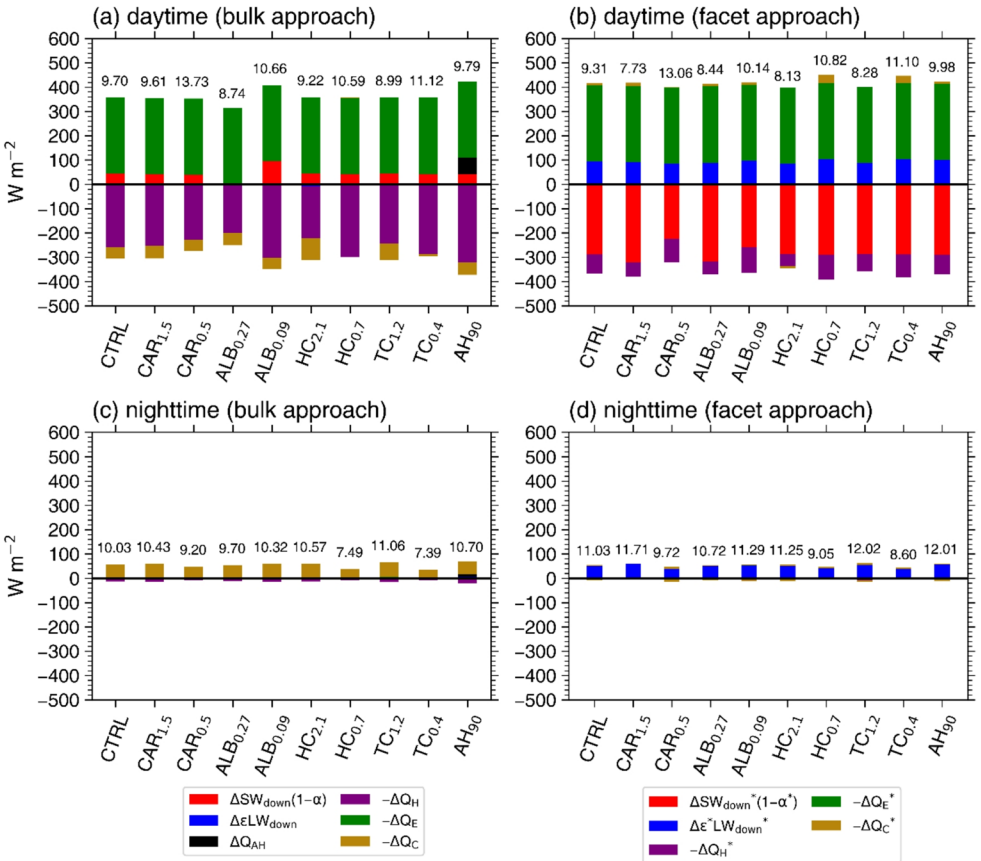

Fig. 9 (**a**, **c**) Same as Fig. 7a except for the sensitivity experiments of $CAR_{1.5}$, $CAR_{0.5}$, $ALB_{0.27}$, $ALB_{0.09}$, $HC_{2.1}$, $HC_{0.7}$, $TC_{1.2}$, $TC_{0.4}$, and AH_{90}. (**b**, **d**) Same as Fig. 7b except for the sensitivity experiments of $CAR_{1.5}$, $CAR_{0.5}$, $ALB_{0.27}$, $ALB_{0.09}$, $HC_{2.1}$, $HC_{0.7}$, $TC_{1.2}$, $TC_{0.4}$, and AH_{90}

The increases in heat capacity and thermal conductivity of urban facets decrease both $SUHII_{bulk}$ and $SUHII_{facet}$ during the daytime but increase both $SUHII_{bulk}$ and $SUHII_{facet}$ during the nighttime. Compared with the $HC_{0.7}$ experiment, in the $HC_{2.1}$ experiment, the daytime mean $SUHII_{bulk}$ ($SUHII_{facet}$) is weaker by 1.37 (2.68) °C and the nighttime mean $SUHII_{bulk}$ ($SUHII_{facet}$) is stronger by 3.07 (2.20) °C. In the $TC_{1.2}$ experiment, the daytime mean $SUHII_{bulk}$ ($SUHII_{facet}$) is weaker by 2.13 (2.82) °C and the nighttime mean $SUHII_{bulk}$ ($SUHII_{facet}$) is stronger by 3.67 (3.42) °C compared with the $TC_{0.4}$ experiment. In both bulk and facet approaches, the most noticeable change responsible for the changes in SUHI intensity with the heat capacity or thermal conductivity of urban facets appears in the urban-rural difference in storage heat flux. The changes in the daytime and nighttime $-\Delta Q_C$ ($-\Delta Q_C^*$) with the increase in heat capacity or thermal conductivity of urban facets cause the decrease in daytime $SUHII_{bulk}$ ($SUHII_{facet}$) and the increase in nighttime $SUHII_{bulk}$ ($SUHII_{facet}$), respectively.

The inclusion of anthropogenic heat increases both $SUHII_{bulk}$ and $SUHII_{facet}$ during the daytime and nighttime. Compared with the control experiment, in the AH_{90} experiment, the daytime mean $SUHII_{bulk}$ ($SUHII_{facet}$) is stronger by 0.09 (0.68) °C and the nighttime mean $SUHII_{bulk}$ ($SUHII_{facet}$) is stronger by 0.66 (0.98) °C. The most noticeable change responsible for the increases in daytime and nighttime $SUHII_{bulk}$ appears in ΔQ_{AH}, while that for the increases in daytime and nighttime $SUHII_{facet}$ appears in $\Delta\varepsilon^* LW_{down}{}^*$. Both $SUHII_{bulk}$ and $SUHII_{facet}$ somewhat vary with the changes in urban-parameter values. Nonetheless, Fig. 9 indicates that the main causes of SUHIs in each of the bulk and facet approaches found from the control experiment also hold for the urban-parameter sensitivity experiments.

Finally, it is worthwhile to mention that for very small canyon aspect ratios for which the area of vertical walls is very small, the main causes of nighttime SUHIs in the bulk and facet approaches are the same. Figure 10 is the same as Fig. 7 except for the sensitivity experiment with a canyon aspect ratio of 0.1. In this rather extreme case, the daytime $SUHII_{bulk}$ and $SUHII_{facet}$ are considerably stronger and the nighttime $SUHII_{bulk}$ and $SUHII_{facet}$ are considerably weaker than in the control experiment. Interestingly, in both approaches, the urban-rural difference in storage heat flux is the most important cause of the nighttime SUHI. In the bulk approach, $-\Delta Q_C$ is predominant during the nighttime as in

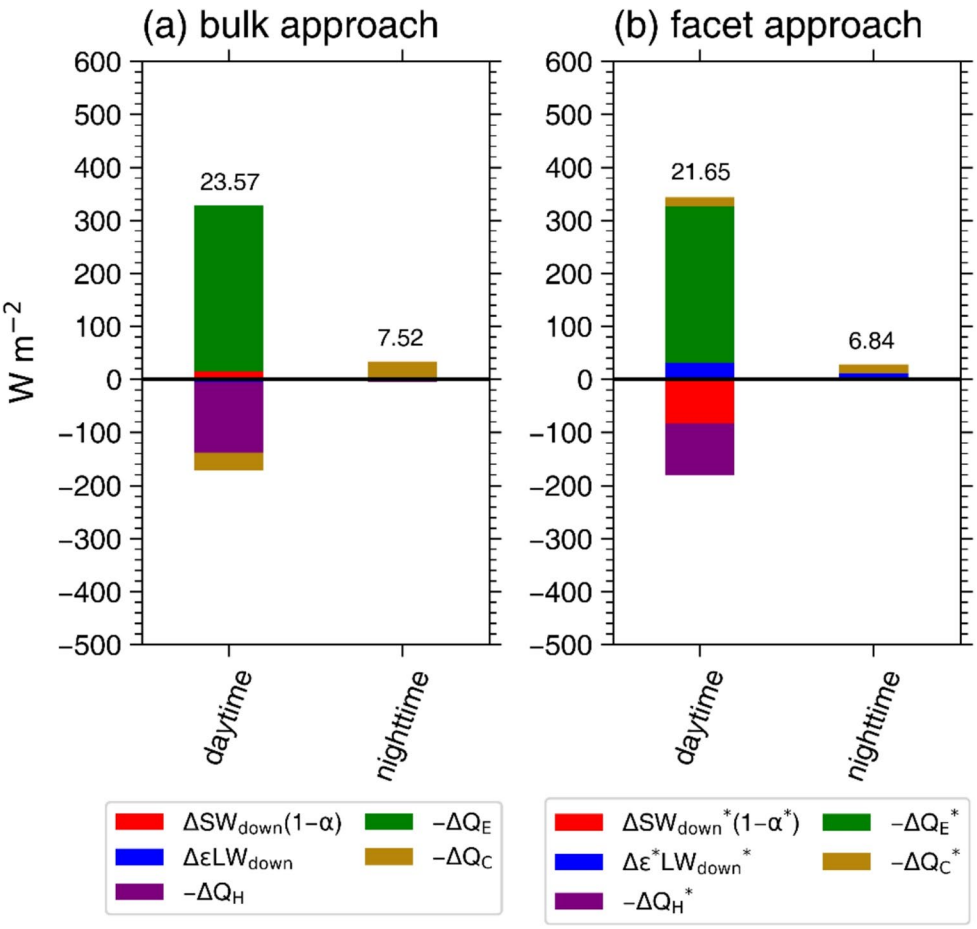

Fig. 10 Same as Fig. 7 except for the sensitivity experiment with a canyon aspect ratio of 0.1

other experiments, the nighttime mean $-\Delta Q_C$ being 29.8 W m^{-2}. In the facet approach, the nighttime mean $-\Delta Q_C{}^*$ (17.1 W m^{-2}) is larger than the nighttime mean $\Delta\varepsilon^* LW_{down}{}^*$ (10.9 W m^{-2}), unlike other experiments. These results indicate that as the urban surface flattens, the surface energy fluxes in the bulk approach becomes similar to those in the facet approach.

4 Summary and conclusions

This study examines the causes of SUHIs using a UCM coupled with the WRF model. The urban surface temperature is represented by the area-weighted average of individual facet surface temperatures. Corresponding to the urban surface temperature, the area-weighted averages of individual facet energy fluxes simulated by the UCM are calculated and compared with rural surface energy fluxes (facet approach). This facet approach is different from the conventional approach in which the urban surface energy fluxes that satisfy the energy balance for an urban conceptual volume, also simulated by the UCM, are compared with rural surface energy fluxes (bulk approach). In this bulk approach, the urban surface energy fluxes are represented at the top surface of the conceptual volume and thus the representative urban surface temperature for them is the radiative surface temperature inverted from emitted longwave radiation at the top surface of the conceptual volume.

Two-dimensional idealized ensemble simulations are carried out, which roughly represent mid-latitude hot and dry summer conditions. In both bulk and facet approaches, the daytime SUHI is primarily attributed to less evapotranspiration in the urban area. However, the bulk and facet approaches yield contrasting results for several other factors affecting the daytime SUHI. For example, in the bulk approach, the urban-rural difference in net shortwave radiation is interpreted as a factor intensifying the daytime SUHI because the multiple reflections occurring within the urban canyon cause the downward shortwave radiation to be more absorbed within the urban conceptual volume than at the rural surface. On the other hand, in the facet approach, the urban-rural difference in net shortwave radiation is interpreted as a factor weakening the daytime SUHI because the mean amount of shortwave radiation absorbed by individual facets is smaller than that absorbed by the rural surface due to the shade within the urban canyon. In the bulk approach, the primary cause of the nighttime SUHI is found to be larger urban heat storage in the urban area. On the other hand, in the facet approach, the primary cause of the nighttime SUHI is found to be the trapping of longwave radiation within the urban canyon. The differences in the causes of SUHIs between the bulk and facet approaches are robust for changes in physics parameterization schemes and some changes in urban-parameter values. Interestingly, for a very small canyon aspect ratio (e.g., $H_{build}/W_{road} = 0.1$), both approaches yield the same main cause of the nighttime SUHI.

In this study, we reveal that the causes of SUHIs can be interpreted differently depending on how the urban surface energy balance is represented using the surface energy fluxes simulated by a UCM. Moreover, this study suggests that the facet approach, which considers surface energy fluxes better corresponding to the thermodynamic urban surface temperature (facet surface temperatures), provides more physically consistent framework than the conventional bulk approach for exploring the reason why the urban physical surfaces are warmer than the rural surfaces (i.e., SUHI causes). Future investigations into the SUHI causes using the facet approach for various cities with different geographical settings and background climates will help to deepen the understanding of SUHIs.

The facet surface temperatures used to define the SUHI in this study represent actual thermodynamic conditions of urban surface. However, the facet surface temperatures are difficult to be in-situ measured for a whole city (Morrison et al. 2018; Gawuc et al. 2022). Satellite observations can provide the facet surface temperatures over large spatial extents, but they suffer from their limited abilities to detect three-dimensional urban surfaces and biases depending on view angles (Krayenhoff and Voogt 2016; Du et al. 2023). These make it hard to well verify the facet surface temperatures simulated by a UCM against observations. To better examine SUHIs and their causes using facet surface temperatures for various cities, it is necessary to better observe/estimate the facet surface temperatures (Yang et al. 2021; Klimenka et al. 2025).

In this study, which of the urban-rural differences in radiative, turbulent, and storage heat fluxes is mainly responsible for the urban-rural difference in emitted longwave radiation is analyzed to investigate the causes of SUHIs. However, it should be noted that the emitted longwave radiation is closely associated not only with the surface temperature but also with the surface emissivity. Decomposing the urban-rural difference in emitted longwave radiation into the contribution of the urban-rural difference in surface temperature (SUHI) and that of the urban-rural difference in surface emissivity could provide further insights into the causes of SUHIs.

Finally, this study considers the rural area covered by cropland/woodland (low vegetation) and uses the Noah land surface model with bulk surface treatment where the rural surface temperature and rural surface energy fluxes are treated in the same way in the bulk and facet approaches. However, for rural areas covered by high vegetation, the rural surface temperature and rural surface energy fluxes

might differ in the bulk and facet approaches. To better examine the causes of SUHIs under various rural configurations in the facet approach, applying a similar facet approach to rural areas is needed using a more sophisticated land surface model that can treat vegetation canopies (e.g., Niu et al. 2011).

Acknowledgements The authors are grateful to two anonymous reviewers who provided valuable comments on this work.

Author contributions Jong-Jin Baik designed this study. Kyeongjoo Park performed the data analysis and visualization and wrote the original manuscript. Jong-Jin Baik and Han-Gyul Jin reviewed and edited the manuscript. All authors discussed the results. All authors read and approved the final version of the manuscript.

Funding Kyeongjoo Park and Jong-Jin Baik were supported by the National Research Foundation of Korea (NRF) under grant RS-2025-00562044. Han-Gyul Jin was supported by Learning & Academic research institution for Master's·PhD students, and Postdocs (LAMP) Program of the National Research Foundation of Korea (NRF) grant funded by the Ministry of Education (No. RS-2023-00301938).

Data availability The datasets generated during the current study are available from the corresponding authors upon request.

Code availability The codes used for analyses in this study are available from the corresponding authors upon request.

Declarations

Ethics approval Not applicable.

Consent for publication Not applicable.

Consent to participate Not applicable.

Competing interests The authors declare no competing interests.

References

Arnfield AJ (2003) Two decades of urban climate research: a review of turbulence, exchanges of energy and water, and the urban heat island. Int J Climatol 23:1–26

Cao C, Lee X, Liu S, Schultz N, Xiao W, Zhang M, Zhao L (2016) Urban heat islands in China enhanced by haze pollution. Nat Commun 7:12509

Chang Y, Xiao J, Li X, Middel A, Zhang Y, Gu Z, Wu Y, He S (2021) Exploring diurnal thermal variations in urban local climate zones with ECOSTRESS land surface temperature data. Remote Sens Environ 263:112544

Chen F, Dudhia J (2001) Coupling an advanced land surface–hydrology model with the Penn State–NCAR MM5 modeling system. Part I: model implementation and sensitivity. Mon Weather Rev 129:569–585

Chen F, Kusaka H, Bornstein R, Ching J, Grimmond CSB, Grossman-Clarke S, Loridan T, Manning KW, Martilli A, Miao S, Sailor D, Salamanca FP, Taha H, Tewari M, Wang X, Wyszogrodzki AA, Zhang C (2011) The integrated WRF/urban modelling system: development, evaluation, and applications to urban environmental problems. Int J Climatol 31:273–288

Chen F, Yang X, Zhu W (2014) WRF simulations of urban heat island under hot-weather synoptic conditions: the case study of Hangzhou City, China. Atmos Res 138:364–377

Chew LW, Liu X, Li X-X, Norford LK (2021) Interaction between heat wave and urban heat island: a case study in a tropical coastal city, Singapore. Atmos Res 247:105134

Deilami K, Kamruzzaman M, Liu Y (2018) Urban heat island effect: a systematic review of spatio-temporal factors, data, methods, and mitigation measures. Int J Appl Earth Obs Geoinf 67:30–42

Du H, Zhan W, Liu Z, Krayenhoff ES, Chakraborty TC, Zhao L, Jiang L, Dong P, Li L, Huang F, Wang S, Xu Y (2023) Global mapping of urban thermal anisotropy reveals substantial potential biases for remotely sensed urban climates. Sci Bull 68:1809–1818

Dudhia J (1989) Numerical study of convection observed during the Winter Monsoon Experiment using a mesoscale two-dimensional model. J Atmos Sci 46:3077–3107

Feng L, Tian H, Qiao Z, Zhao M, Liu Y (2020) Detailed variations in urban surface temperatures exploration based on unmanned aerial vehicle thermography. IEEE J Sel Top Appl Earth Obs Remote Sens 13:204–216

Fitria R, Kim D, Baik J, Choi M (2019) Impact of biophysical mechanisms on urban heat island associated with climate variation and urban morphology. Sci Rep 9:19503

Fortuniak K (2008) Numerical estimation of the effective albedo of an urban canyon. Theor Appl Climatol 91:245–258

Garuma GF (2018) Review of urban surface parameterizations for numerical climate models. Urban Clim 24:830–851

Gawuc L, Łobocki L, Strużewska J (2022) Application of the profile method for the estimation of urban sensible heat flux using roadside weather monitoring data and satellite imagery. Urban Clim 42:101098

Grimmond CSB, Blackett M, Best MJ, Barlow J, Baik J-J, Belcher SE, Bohnenstengel SI, Calmet I, Chen F, Dandou A, Fortuniak K, Gouvea ML, Hamdi R, Hendry M, Kawai T, Kawamoto Y, Kondo H, Krayenhoff ES, Lee S-H, Loridan T, Martilli A, Masson V, Miao S, Oleson K, Pigeon G, Porson A, Ryu Y-H, Salamanca F, Shashua-Bar L, Steeneveld GJ, Tombrou M, Voogt J, Young D, Zhang N (2010) The international urban energy balance models comparison project: first results from phase 1. J Appl Meteorol Climatol 49:1268–1292

Hamdi R, Schayes G (2008) Sensitivity study of the urban heat island intensity to urban characteristics. Int J Climatol 28:973–982

Han J-Y, Baik J-J (2008) A theoretical and numerical study of urban heat island–induced circulation and convection. J Atmos Sci 65:1859–1877

Harmay NSM, Kim D, Choi M (2021) Urban Heat Island associated with Land Use/Land Cover and climate variations in Melbourne, Australia. Sust Cities Soc 69:102861

Heaviside C, Macintyre H, Vardoulakis S (2017) The Urban Heat Island: implications for health in a changing environment. Curr Environ Health Rep 4:296–305

Hong S-Y, Lim J-OJ (2006) The WRF single-moment 6-class microphysics scheme (WSM6). J Korean Meteorol Soc 42:129–151

Hong S-Y, Noh Y, Dudhia J (2006) A new vertical diffusion package with an explicit treatment of entrainment processes. Mon Weather Rev 134:2318–2341

Hong S-H, Jin H-G, Han J-Y, Baik J-J (2024) Initiation and evolution of urban-induced precipitation under different background wind speeds: roles of urban breeze circulation and cold pool. Theor Appl Climatol 155:9457–9470

Iacono MJ, Delamere JS, Mlawer EJ, Shephard MW, Clough SA, Collins WD (2008) Radiative forcing by long-lived greenhouse gases: calculations with the AER radiative transfer models. J Geophys Res Atmos 113:D13103

Imhoff ML, Zhang P, Wolfe RE, Bounoua L (2010) Remote sensing of the urban heat island effect across biomes in the continental USA. Remote Sens Environ 114:504–513

Janjić ZI (1994) The step-mountain eta coordinate model: further developments of the convection, viscous sublayer, and turbulence closure schemes. Mon Weather Rev 122:927–945

Jiménez PA, Dudhia J, González-Rouco JF, Navarro J, Montávez JP, García-Bustamante E (2012) A revised scheme for the WRF surface layer formulation. Mon Weather Rev 140:898–918

Kanda M (2007) Progress in urban meteorology: a review. J Meteorol Soc Jpn 85B:363–383

Klemp JB, Dudhia J, Hassiotis AD (2008) An upper gravity-wave absorbing layer for NWP applications. Mon Weather Rev 136:3987–4004

Klimenka M, Zhao K, Hilland R, Zhang F, Voogt J, Ratti C (2025) Instant infrared: estimating urban surface temperatures from street view imagery. Build Environ 267:112122

Krayenhoff ES, Voogt JA (2016) Daytime thermal anisotropy of urban neighbourhoods: morphological causation. Remote Sens 8:108

Krayenhoff ES, Christen A, Martilli A, Oke TR (2014) A multi-layer radiation model for urban neighbourhoods with trees. Bound-Layer Meteorol 151:139–178

Kusaka H, Kondo H, Kikegawa Y, Kimura F (2001) A simple single-layer urban canopy model for atmospheric models: comparison with multi-layer and slab models. Bound-Layer Meteorol 101:329–358

Lai J, Zhan W, Huang F, Voogt J, Bechtel B, Allen M, Peng S, Hong F, Liu Y, Du P (2018) Identification of typical diurnal patterns for clear-sky climatology of surface urban heat islands. Remote Sens Environ 217:203–220

Li C, Zhang N (2021) Analysis of the daytime urban heat island mechanism in East China. J Geophys Res Atmos 126:e2020JD034066

Li D, Liao W, Rigden AJ, Liu X, Wang D, Malyshev S, Shevliakova E (2019) Urban heat island: aerodynamics or imperviousness? Sci Adv 5:eaau4299

Li C, Zhang N, Ren K, Zhao W, Wu J, Sun Y (2024) Biophysical drivers of seasonal hysteresis of urban heat islands across climates and urban landscapes. J Geophys Res Atmos 129:e2023JD040446

Martilli A (2007) Current research and future challenges in urban mesoscale modelling. Int J Climatol 27:1909–1918

Masson V, Lemonsu A, Hidalgo J, Voogt J (2020) Urban climates and climate change. Annu Rev Environ Resour 45:411–444

Miao S, Chen F, LeMone MA, Tewari M, Li Q, Wang Y (2009) An observational and modeling study of characteristics of urban heat island and boundary layer structures in Beijing. J Appl Meteorol Climatol 48:484–501

Mills G (2014) Urban climatology: history, status and prospects. Urban Clim 10:479–489

Mlawer EJ, Taubman SJ, Brown PD, Iacono MJ, Clough SA (1997) Radiative transfer for inhomogeneous atmospheres: RRTM, a validated correlated-k model for the longwave. J Geophys Res Atmos 102:16663–16682

Morrison W, Kotthaus S, Grimmond CSB, Inagaki A, Yin T, Gastellu-Etchegorry J-P, Kanda M, Merchant CJ (2018) A novel method to obtain three-dimensional urban surface temperature from ground-based thermography. Remote Sens Environ 215:268–283

Niu G-Y, Yang Z-L, Mitchell KE, Chen F, Ek MB, Barlage M, Kumar A, Manning K, Niyogi D, Rosero E, Tewari M, Xia Y (2011) The community Noah land surface model with multiparameterization options (Noah-MP): 1. Model description and evaluation with local-scale measurements. J Geophys Res Atmos 116:D12109

Oke TR (1988) The urban energy balance. Prog Phys Geogr 12:471–508

Oke TR, Mills G, Christen A, Voogt JA (2017) Urban climates. Cambridge University Press, Cambridge

Qian Y, Chakraborty TC, Li J, Li D, He C, Sarangi C, Chen F, Yang X, Leung LR (2022) Urbanization impact on regional climate and extreme weather: current understanding, uncertainties, and furture research directions. Adv Atmos Sci 39:819–860

Ramamurthy P, Bou-Zeid E, Smith JA, Wang Z, Baeck ML, Saliendra NZ, Hom JL, Welty C (2014) Influence of subfacet heterogeneity and material properties on the urban surface energy budget. J Appl Meteorol Climatol 53:2114–2129

Ryu Y-H, Baik J-J (2012) Quantitative analysis of factors contributing to urban heat island intensity. J Appl Meteorol Climatol 51:842–854

Ryu Y-H, Baik J-J, Lee S-H (2011) A new single-layer urban canopy model for use in mesoscale atmospheric models. J Appl Meteorol Climatol 50:1773–1794

Saher R, Stephen H, Ahmad S (2021) Understanding the summertime warming in canyon and non-canyon surfaces. Urban Clim 38:100916

Sarrat C, Lemonsu A, Masson V, Guedalia D (2006) Impact of urban heat island on regional atmospheric pollution. Atmos Environ 40:1743–1758

Shen P, Zhao S, Ma Y (2021) Perturbation of urbanization to Earth's surface energy balance. J Geophys Res Atmos 126:e2020JD033521

Shi Z, Yang J, Wang L-e, Lv F, Wang G, Xiao X, Xia J (2022) Exploring seasonal diurnal surface temperature variation in cities based on ECOSTRESS data: a local climate zone perspective. Front Public Health 10:1001344

Skamarock WC, Klemp JB, Dudhia J, Gill DO, Liu Z, Berner J, Wang W, Powers JG, Duda MG, Barker DM, Huang X-Y (2019) A description of the advanced research WRF model version 4. National Center for Atmospheric Research, Colorado

Song B, Park K (2014) Validation of ASTER surface temperature data with in situ measurements to evaluate heat islands in complex urban areas. Adv Meteorol 2014:620410

Stewart ID, Mills G (2021) The urban heat island. Elsevier, Amsterdam

Stewart ID, Krayenhoff ES, Voogt JA, Lachapelle JA, Allen MA, Broadbent AM (2021) Time evolution of the surface urban heat island. Earth's Future 9:e2021EF002178

Sugawara H, Takamura T (2014) Surface albedo in cities: case study in Sapporo and Tokyo, Japan. Bound-Layer Meteorol 153:539–553

Tabassum A, Hong S-H, Park K, Baik J-J (2024) Impacts of changes in soil moisture on urban heat islands and urban breeze circulations: idealized ensemble simulations. Asia-Pac J Atmos Sci 60:541–553

Taha H (1997) Urban climates and heat islands: albedo, evapotranspiration, and anthropogenic heat. Energy Build 25:99–103

Theeuwes NE, Steenveld GJ, Ronda RJ, Heusinkveld BG, van Hove LWA, Holtslag AAM (2014) Seasonal dependence of the urban heat island on the street canyon aspect ratio. Q J R Meteorol Soc 140:2197–2210

Tsiringakis A, Holtslag AAM, Grimmond S, Steeneveld GJ (2020) Surface and atmospheric driven variability of the single-layer urban canopy model under clear-sky conditions over London. J Geophys Res Atmos 125:e2019JD032167

Voogt JA, Oke TR (1997) Complete urban surface temperatures. J Appl Meteorol Climatol 36:1117–1132

Wang L, Li D (2021) Urban heat islands during heat waves: a comparative study between Boston and Phoenix. J Appl Meteorol Climatol 60:621–641

Wang L, Li D, Zhang N, Sun J, Guo W (2020) Surface urban heat and cool islands and their drivers: an observational study in Nanjing, China. J Appl Meteorol Climatol 59:1987–2000

Yang X, Li Y (2015) The impact of building density and building height heterogeneity on average urban albedo and street surface temperature. Build Environ 90:146–156

Yang J, Shi Q, Menenti M, Wong MS, Wu Z, Zhao Q, Abbas S, Xu Y (2021) Observing the impact of urban morphology and building

geometry on thermal environment by high spatial resolution thermal images. Urban Clim 39:100937

Zhao L, Lee X, Smith RB, Oleson K (2014) Strong contributions of local background climate to urban heat islands. Nature 511:216–219

Zhao L, Oppenheimer M, Zhu Q, Baldwin JW, Ebi KL, Bou-Zeid E, Guan K, Liu X (2018) Interactions between urban heat islands and heat waves. Environ Res Lett 13:034003

Zhou D, Xiao J, Bonafoni S, Berger C, Deilami K, Zhou Y, Frolking S, Yao R, Qiao Z, Sobrino JA (2018) Satellite remote sensing of surface urban heat islands: progress, challenges, and perspectives. Remote Sens 11:48